Sensors & Actuators: B. Chemical 460 (2026) 139921

Contents lists available at ScienceDirect

Sensors and Actuators: B. Chemical

journal homepage: www.elsevier.com/locate/snb

Discrimination between healthy and tomato spotted wilt virus infected tomato plants by means of temperature-modulated gas sensors

Carlo Pennacchio [a,b,*], Niccolò Miotti [c], Massimo Turina [c], Marina Ciuffo [c], Emanuela Gobbi [d], Moez Maghrebi [e], Simone Bossi [e], Gianpiero Vigani [e], Guido Faglia [a,b], Camilla Baratto [a,b], Andrea Ponzoni [a,b,*]

[a] CNR-INO (National Research Council – National Institute of Optics), Brescia Unit, Via Branze 45, Brescia 25123, Italy
[b] Department of Information Engineering, University of Brescia, Via Branze 38, Brescia 25123, Italy
[c] CNR-IPSP (National Research Council - Institute for Sustainable Plants Protection), Strada delle Cacce 73, Torino 10135, Italy
[d] Department of Molecular and Translational Medicine, University of Brescia, Viale Europa 11, Brescia 25123, Italy
[e] Department of Life Sciences and Systems Biology, University of Turin, Innovation center, Via Quarello 15/A, Torino 10135, Italy

ARTICLE INFO

Keywords:
Metal oxide gas sensors
Temperature modulation
Tomato spotted wilt virus
Tomato plants

ABSTRACT

Plant virus diseases represent a major issue in agriculture, with relevant economic impact. The correlation between the plant health status and the emission of characteristics volatiles has been well established in the literature of analytical chemistry. However, the development of a cost-affordable technology suitable to work in-field for the automatic detection of these olfactive signals remains a major challenge in gas sensing. In this work, we investigated the use of metal oxide gas sensors working with temperature modulation to detect the outbreak of tomato spotted wilt virus infection in tomato plants, chosen as a relevant case study. To handle sensor-to-sensor reproducibility issues and plants' individualities we designed experiments comprising 8 plants per time, each equipped with a dedicated sensor. Considering the complex time dependence of plants' emissions and infection-independent interfering effects, we adopted an analysis method exploiting the signals from the whole network. Results indicates that the proposed technology detects the outbreak of infection through the detection of an anomalous signals from individual sensors with respect to the common behavior of the network, and is potentially suitable for autonomous, non-invasive, in-field operation. Polymerase Chain Reaction and Gas-Chromatography Mass-Spectroscopy characterizations suggest that the sensing system respond mainly to volatiles of plant tissues damage. These results indicate the potentialities of this technology for the development of a distributed network aimed at a non-invasive monitoring of plants health status in greenhouses.

1. Introduction

The automatic and early detection of virus-infected plants inside greenhouses or even in open field through a distribute network of cheap sensors would be a great economic and technological advancement. This would allow to drastically reduce the crop damage by taking countermeasures to limit the infection spread. To give an idea of the economic burden, in 2014 plant virus pandemics and epidemics were estimated to have a global impact of more than USD 30 billion [1]. Sensing the volatile organic compounds (VOCs) emitted by infected plants is a promising route to accomplish this task. Indeed, it has been well documented that plants emit a broad spectrum of VOCs upon biotic and abiotic stresses [2,3]. The emitted volatilome is a complex mixture of several VOCs, including terpenes, alcohols, esters, aldehydes, whose concentrations feature time dependence, reflecting the different stages of the metabolic response of the plant and environmental condition variations [4–6]. Methyl salicylate (MeSa) is widely reported as marker of biotic and abiotic plant stress [7–9], its release starting a few hours after inoculation and reaching a peak within a couple of days [7]. However, these results have been recorded by means of very efficient, but expensive, laboratory techniques such as Gas Chromatography coupled with Mass spectrometry (GC/MS) and Proton Transfer Reaction (PTR). Achieving these results with cheap and portable instrumentation suitable for in-field operation remains a major challenge. Indeed, MeSa concentration lies in the low ppb range [7], which is quite hard to detect for most of solid-state gas sensors, particularly in real scenarios. The

* Corresponding authors at: CNR-INO (National Research Council – National Institute of Optics), Brescia Unit, Via Branze 45, Brescia 25123, Italy.
E-mail addresses: carlo.pennacchio01@universitadipavia.it (C. Pennacchio), andrea.ponzoni@cnr.it (A. Ponzoni).

https://doi.org/10.1016/j.snb.2026.139921
Received 3 December 2025; Received in revised form 24 February 2026; Accepted 4 April 2026
Available online 6 April 2026

detection of VOCs originating from necrosis and tissue damages looks more feasible. Their concentration may reach the order of 10 ppm in case of severe infection, accounting for the contributions of volatile products from the lipoxygenase pathway (LOX products, due to leaf membrane degradation) and monoterpenes (due to glandular trichomes degradation) [10].

Considering the complex composition of the target atmosphere, the electronic nose (EN) technology, which is based on a sensor array with broad sensitivity and a pattern recognition software [11,12], is promising. Metal oxide (MOX) gas sensors are among the widest explored devices for the development of electronic noses, owing to their reduced size and power consumption, their mechanical and chemical robustness, as well as the possibility to tune their sensing properties over a wide range, which can be done by properly designing the sensing material [13–15] and its activation method, namely the working temperature or UV-light exposure [16–19].

To cite some relevant examples in agritech applications, Zhou et al. and Ghaffari et al. used a commercial EN coupled with a custom headspace sampling system to spot rice plants attacked by *Nilaparvata lugens* [20], and tomato plants infected by powdery mildew (*Oidium lycopersicum*) and spider mite [21]. Cellini et al. [22] tested commercial sensing systems with the aim of detecting bacterial infections of *Erwinia amylovora* and *Pseudomonas syringae pv. syringae* on apple plants. Cui et al. [23] built a custom EN optimized for the diagnosis of aphid-stressed tomato plants. The EN technology revealed also successful in discriminating between non-infested and emerald ash borer infested trees on the basis of volatiles emitted by the tree sapwoods [24]. In all the above-mentioned papers, bulky systems have been used, which are not suitable to work in-field in a distributed network. Moreover, these ENs use a source of clean air as a reference, which is readily available in the laboratory but may be hardly compatible with in-site operation. Temperature modulation is a promising approach to solve these issues. Since the reaction rates of analyte gases vary with temperature, a cyclic variation of the working temperature can give a unique signature for each gas through the sensor resistance vs time curve, $R_s(t)$, which can be used as input of the pattern recognition software [25]. This approach reveled suitable to address selectively for different target gases, both diluted one-by-one in air [26,27] and mixed in complex blends [27–29]. Selectivity in presence of varying levels of humidity was also demonstrated [30,31]. In principle, the temperature modulation mode allows to develop a compact sensing system based on a single gas sensor. Moreover, since the device response is related to the shape of the $R_s(t)$ curve instead of a single resistance value, the use of a reference air is not necessary [32,33]. This means that the sensing system do not need to recover any baseline, the rate of its output is thus only limited by the thermal period, and it may be considered an almost real time monitoring. Further considering the small size typical of temperature-modulated metal-oxide gas sensors, these features are fundamental for the realization of a network of sensing systems distributed over the greenhouse area.

In this paper we investigated a prototypal network of lightweight and cheap sensors exploiting temperature modulation as a possible technological solution for automatic detection of infected plants inside a greenhouse. In particular, we have used *Solanum lycopersicum* L. cv. Marmande plants and tomato spotted wilt virus (TSWV) as pathogen. In view of the possible exploitation as a distributed network of devices, accounting for sensor reproducibility between nominally identical devices and differences between individual plants is a fundamental issue. To this aim, we designed our experiments with 8 replicas (every session involves 8 tomato plants, each equipped with a dedicated sensor device). Our work indicates that, upon a proper data analysis, information about the health status of the plants emerges over strong interfering effects arising from environmental and plant transpiration effects that are intrinsic in this application. Results highlight the potentialities of this technology for the development of a distributed network aimed at a non-invasive monitoring of plants health status in greenhouses.

2. Materials and methods

2.1. Sensors and data acquisition

Our Sensing system was composed by a compact (size is about 25 mm×90 mm x 10 mm), USB-controlled, data acquisition platform (MOXstick by JLM Innovation GmbH, [34]), equipped with a single metal-oxide (MOX) gas sensor (TGS 2620 by Figaro USA Inc.).

Temperature modulation was used with a thermal period of 50 s. The heater voltage was kept at 3 V for 25 s (cold semi-period) and at 4 V for the remaining 25 s (hot semi-period). The data acquisition sampling time was set to 0.5 s. As an example, Fig. 1 reports the voltage applied to the heater and the sensor resistance vs time curve acquired in the headspace of a healthy plant. To resume the shape of this curve, for each thermal period we extrapolated a set of 14 parameters working as input features for data analysis. As detailed in Supplementary Material, 1, data pre-processing and feature selection were applied to reduce noise and work with relevant (not redundant) features. Selected features are listed in Table 1.

To monitor the temperature (T) and relative humidity (RH) inside the bottles (setup details are in 3), we used a combined RH/T sensor (TSP01B by Thorlabs Inc.). The sampling time was 50 s to match the thermal period of the MOX devices.

2.2. Plants growth, inoculation and genetic diagnosis of infection

Tomato plants (*S. lycopersicum* L. cv. Marmande) were cultivated in a growth chamber under controlled conditions, namely a 16/8-hour day/night photoperiod, of 25 °C and 18 °C day/night temperatures, and 70% relative humidity. Three-week-old plants were mechanically inoculated with the TSWV isolate I244 (PLAVIT collection). The inoculum was prepared from freshly infected leaves of *Nicotiana benthamiana*, which were homogenized in an inoculation buffer containing 0.05 M potassium phosphate buffer (pH 7.0), 1 mM EDTA, 5 mM DIECA, and 5 mM thioglycolic acid. Carborundum (600 mesh) was used as an abrasive agent to facilitate inoculation, and the leaves were rinsed with water immediately after inoculation. Mock-inoculated plants were inoculated with an extract of a healthy leaf.

At the end of each measuring session, a single leaf from each experimental tomato plant was harvested, and a crude sap extract was obtained using the method described in [35]. Subsequently, 5 µL of the crude extract was boiled in 50 µL of RNase-free water for 5 min. One-step Reverse Transcription quantitative Polymerase Chain Reaction (RT-qPCR) was performed using primers and probes as described in

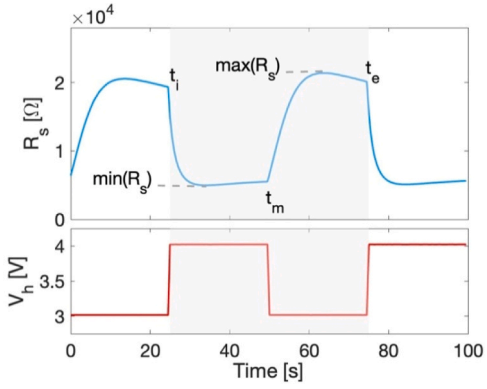

Fig. 1. Time dependence of the sensor resistance (R_s) and of the corresponding squared wave voltage applied to the heater (V_h) to modulate the sensor temperature. The shaded central area highlights an individual thermal period. The extreme values of R_s and the times delimiting the hot (t_i and t_m) and the cold (t_m and t_e) thermal periods are reported as a reference for the selected features listed in Table 1.

Table 1
List of the selected sensor features extracted from the sensor resistance vs time curve for each thermal period. The description refers to Fig. 1.

Sensor feature	Feature description
f_1	R_s variation during the transition from the cold to the hot semiperiod: $R_s(t_i) - min(R_s)$
f_2	R_s variation during the transition from the hot to the cold semiperiod: $Max(R_s) - R_s(t_m)$
f_3	R_s ratio between the transition from the cold to the hot semiperiod: $R_s(t_i) / min(R_s)$
f_4	R_s variation during the cold semiperiod: $R_s(t_m) - min(R_s)$
f_5	R_s ratio during the cold semiperiod: $Max(R_s) / R_s(t_e)$
f_6	Mean value of R_s calculated over the cold semiperiod
f_7	Median value of R_s calculated over the cold semiperiod
f_8	Median value of R_s calculated over the hot semiperiod
f_9	R_s slope, extrapolated from a linear fit applied to the last 5 s of the hot semi-period

[36], with 1 μL of the boiled extract serving as the template. M-MLV Reverse Transcriptase (Thermo Fisher Scientific Inc.) and iTaq Universal Probes Supermix (Bio-Rad Laboratories Inc.) were used for the reverse transcription and PCR reactions, respectively, following the manufacturer instructions.

2.3. VOCs collection and GC/MS analysis

Volatile organic compounds (VOCs) were collected and analyzed using gas chromatography–mass spectrometry (GC–MS). Sampling was carried out in a 12 L modified glass bell jar containing non-flowering tomato plants. The plants were illuminated by an LED fixture providing approximately 170 μmol m^{-2} s^{-1}(corresponding to about 3.74 mW/cm^2) of light under a 16-hour photoperiod. The environmental conditions inside the bell jar were maintained at ~24 °C with 70% relative humidity. The glass bell jar was connected to an aspirating pump via a glass plug with two openings, allowing a continuous flow of ambient air into and out of the jar. Incoming air was filtered through cotton gauze and mixed with the internal environment of the bell jar at a flow rate of 150 mL min^{-1}.

For VOC collection, a Stir Bar Sorptive Extraction (SBSE) system was used to adsorb compounds from the headspace. A polydimethylsiloxane-coated Twister stir bar (0.5 mm thickness, 10 mm length; Gerstel, Germany) was placed in a glass liner connected to the outlet of the bell jar, allowing headspace air to pass over it. Adsorbed VOCs were thermally desorbed from the SBSE using a Gerstel TDU-CIS system. The compounds were cryo-focused at –30 °C before injection and analysis by GC–MS (Agilent 5975 mass spectrometer coupled with an Agilent 6890 N gas chromatograph).

Separation was achieved using a non-polar DB-5MS capillary column (30 m length, 250 μm i.d., 0.25 μm film thickness; 5% phenyl arylene, 95% polydimethylsiloxane). Helium was used as the carrier gas at a constant flow rate of 1.0 mL min^{-1}. The oven temperature program was as follows: initial temperature 60 °C (1 min), ramped at 3.0 °C min^{-1} to 230 °C (2 min), then ramped to 320 °C at 15 °C min^{-1} and held for 5 min.

The mass spectrometer was operated in electron ionization (EI) mode at 70 eV. Acquisition parameters for the quadrupole detector were set in autotune mode, with the ion source at 150 °C and the quadrupole at 230 °C. Mass spectra were acquired over a range of m/z 50–550. VOCs, when present, were identified by comparison of their mass spectra and retention indices (Kováts indices) with reference standards and by matching against the NIST 98 and Adams (2001) libraries using the NIST Mass Spectral Search Program v2.0.

3. Experiment design: setup and specifications

Each experimental session (Fig. 2) consisted of 8 tomato plants (*S. lycopersicum* L. cv. Marmande) placed together over a common saucer inside a climatic chamber (MCT 120 by Angelantoni scientifica, Massa Martana, Italy), set to 25 °C. Four plants out of eight were previously inoculated with TSWV isolate I244, while the other four were mock inoculated. A commercial 3000 K LED strip was mounted inside the chamber and set on in the time interval 6 AM – 21 PM (15 h of light per day and 9 h of darkness), providing an optical power of about 0.25 mW/cm^2, as measured with a photodiode (818-UV by Newport Corp., Irvine, USA); during the day the optical power coming into the chamber from outside was < 200 nW/cm^2. Plants watering was accomplished by a pipe that comes out from the chamber through a hole. Water flowed through the pipe and reached the saucer where the water level was maintained constant at about 3–4 mm. In this way, watering was carried out without opening the thermostatic chamber, which would break the environmental conditions of the experiment.

To keep the volatiles emitted by plants confined as much as possible, each plant was enclosed inside a PET plastic bottle that was fixed to the plant pot through PARAFILM® and duct tape. The soil inside the pot was covered with aluminum foil to avoid the growth of mold and fungi which could alter the VOCs profile inside the bottle. Before sealing the bottle to the pot, a sensing system was placed inside each bottle. As shown in Fig. 2 (B), the sensing system stay suspended at half height of the bottle and doesn't touch the ground. Though this setup is likely to introduce an abiotic stress to plants owing to the reduced air exchange around them, such an additional stress will apply to both healthy and infected plants. Since our study is of comparative type, we may reasonably expect that it will not markedly affect our results. A relative humidity and temperature sensor was introduced (details are in 2.1). All the cables came out from the upper holes of the bottle, ran out of the chamber through a hole and reached the USB port of the PC used for data acquisition. The hole of the chamber was plugged with a cotton pad to prevent the entry of dust and to better maintain temperature inside the chamber.

A webcam was installed inside the climatic chamber to better monitor the course of the disease and to have some time information about symptoms development.

Before the start of the experiment the gas sensors were pre-heated in temperature modulation mode for about 7 days for stabilization in ambient air.

Plants heights and leaves number were noted at the beginning and at the end of each measuring session.

In this paper we present the data obtained in two different experimental sessions, named A and B.

4. Results and discussion

4.1. Genetic diagnosis and plants symptoms

RT-qPCR analysis revealed that in session A zero out of four virus-inoculated plants resulted infected, while in session B, all the four virus-inoculated plants resulted infected at the end of the session. The result of session A is likely due to a low viral titer in the inoculum. Though inoculum was not effective, session A offers an interesting comparative case study with session B, as discussed in 4.

Infection symptoms were further confirmed by visual inspection of plants at the end of each session. In session B, all negative plants increased their height during the experiment and did not present any necrosis on their leaves (Fig. 3 (B) and (C)). Differently, all positive plants did not display any height increase, but exhibited necrosis at the optical microscope investigation, with leaves showing bronzed color (Fig. 3 (B) and (C)), in agreement with previous studies on TSWV infected plants [37]. Severe symptoms were observed in plants B1 and B7, whose leaves showed more abundant necrosis regions with respect

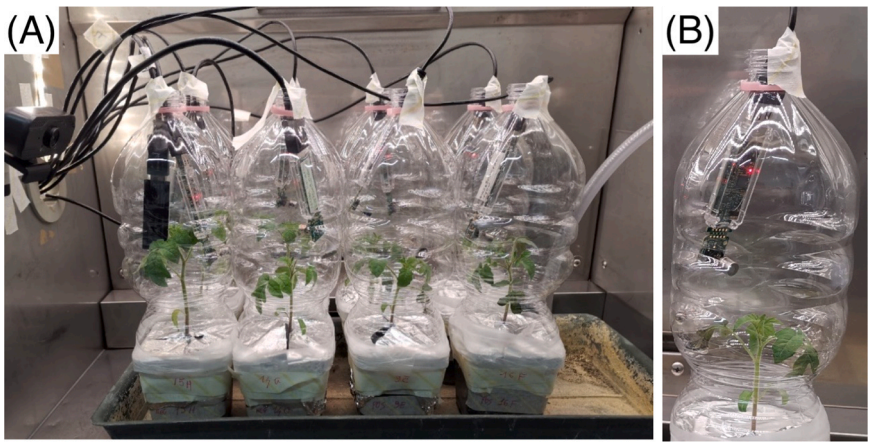

Fig. 2. Pictures of the experimental setup. (A) Setup overview inside the climatic chamber; (B) detail of a sensing system inside a bottle.

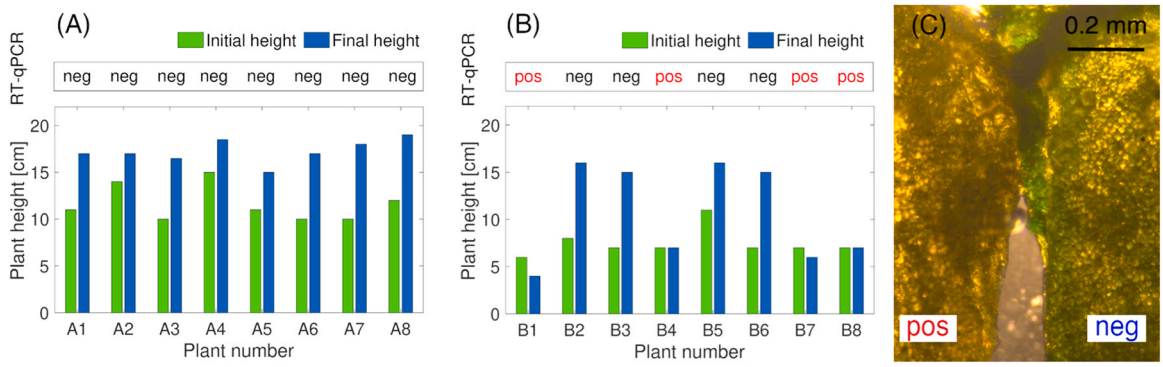

Fig. 3. Plants symptoms and RT-qPCR analysis. Plant heights measured at the beginning and at the end of the experiment and RT-qPCR results acquired at the end of experiment for (A) session A and, (B) session B. (C) optical microscope comparison of leaves from infected (pos) and not-infected (neg) plants of session B.

to other inflected plants of the same session (details are in Supplementary Material, 2). In session A, positive plants did not show any symptoms and were indiscernible from the negative ones, in agreement with the RT-qPCR analysis (Fig. 3 (A)).

The growth of negative plants during experiments and the good status of their leaves indicate that the reduced air circulation of our setup did not appreciably hinder the physiological growth of plants. We may reasonably conclude that virus-induced stress was the most relevant plant stress in our experiments.

4.2. GC/MS analysis

Considering the complex time dependence of volatile emission from plants, GC/MS analysis was carried out collecting the volatiles for a period of 72 h at different times, namely in the temporal ranges of 72 – 144 h and 168 – 240 h since inoculation. No major differences between the chromatograms of control tomato plants and infected plants were detected in the first test, while distinct chromatographic patterns emerged in the second one. As shown in Fig. 4 (A), the volatilome emitted by control plants is composed of 19 different peaks. In contrast, infected plants present a more complex and intense profile. The 19 peaks show an increased intensity, and about 43 additional peaks are present. Among the most abundant compounds, five were identified, namely ethanol 2-butoxy, ethyl octanoate, benzaldehyde, acetophenone and succinic acid ethyl 2-octyl were identified. Over-emission of benzaldehyde and the release of acetophenone are reported in the literature as correlated to biotic stress of tomato plants [6], and as a characteristic emission of wounded leaf in Solanaceae plants [38], respectively.

It is further worth of analyzing the chromatograms sorted by the peak areas, as reported in Fig. 4 (B). Indeed, peak areas are proportional to VOCs concentrations. Though the proportionality factor may vary from compound to compound, variations are usually limited, and the distribution of peak areas can be reasonably considered a good indicator of the gas concentration distribution. Fig. 4 (B) clearly indicate that the target odor is not dominated by a few compounds, but it is composed of a complex and rich blend of VOCs, whose concentration profile is characterized by a long, slowly decaying tail. The sum of the 10 most intense peak areas is almost equal to sum of the remaining tail (peaks from 11th to 62nd).

These results clearly illustrate the complexity of the target odor, whose chemical composition is highly heterogenous, including alcohols, aldehydes, ketones, aromatic compounds and esters, none of these dominating over the others. Because of this, we retain that the sum of compounds, i.e. the whole volatilome, is the target in this application. Accordingly, we chose to work with a MOX sensor featuring a broad sensitivity to alcohols and organic solvents such as the Figaro TGS 2620.

4.3. Overview of sensors data

Fig. 5 reports a brief overview of raw sensors data, namely the $R_s(t)$ curves acquired at two different times of the experimental session B. It shows important effects arising from challenges that are intrinsic of this application and that motivated the data analysis illustrated in Sections 4.4 and 4.5. Challenges may be expected from the working conditions and the small VOCs concentrations released by plants [7]. Indeed, as detailed in Supplementary Material, 3, relative humidity is very large, close to the saturation level, and remains almost constant for the whole duration of experiments. Such a large humidity is known to reduce the

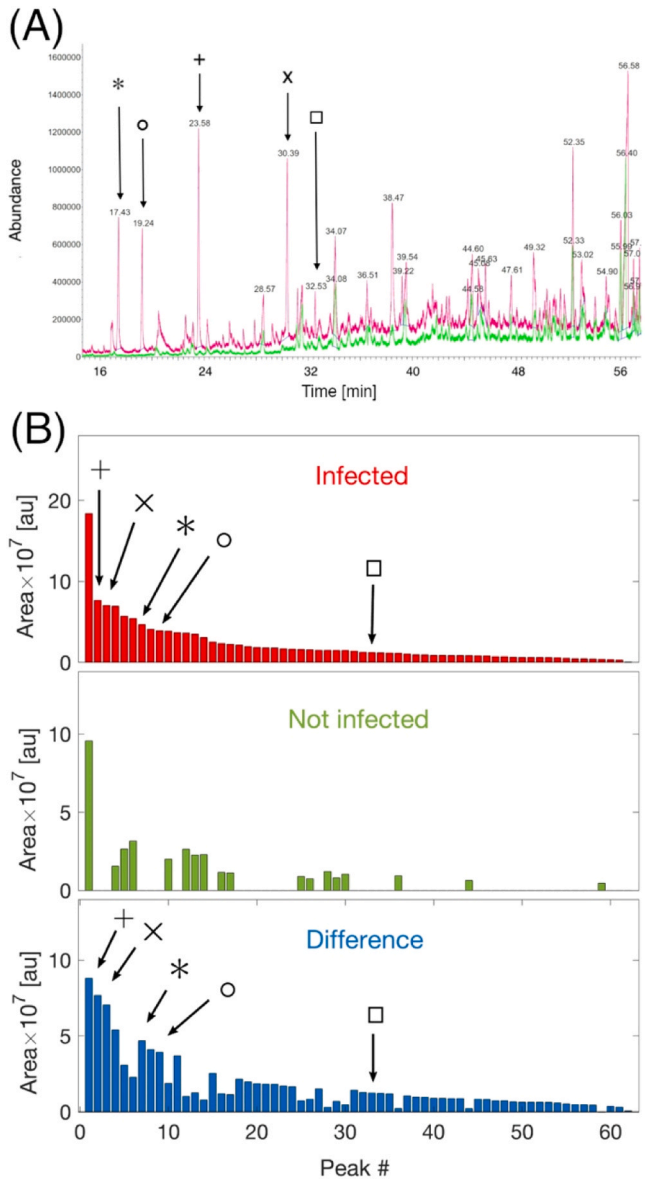

Fig. 4. Analysis of volatiles emitted by infected and not infected plants. (A) GC/MS chromatograms. (B) GC/MS peaks sorted by peak area for infected and not infected plants and their difference. Symbols indicates ethanol 2-butoxy *, ethyl octanoate °, benzaldehyde $^{+}$, acetophenone $^{\times}$, and succinic acid ethyl 2-octyl ester.

sensitivity of MOX-based sensors owing to competing adsorption effects [39]. Though temperature modulation allows for the exploitation of features suitable to mitigate these effects [30,31], their impact is surely relevant. Indeed, the target volatilome is a tiny odor diluted in a large amount of humidity background, which is influenced by both environmental factors and the transpiration of plants. In these conditions, sensor-to-sensor differences that affect metal oxide gas sensors [40], and plant-to-plant variations are likely to become relevant. They may reasonably explain Fig. 5, in which sensors/plants do not group according to the plant health status.

So far, instead of looking for absolute values of the raw sensor data or the related features, we decided to calculate features of the whole sensor network, in contrast to features of individual sensors, and to look for their time evolution, instead of static values. As it will be shown in the next part of the manuscript, this approach will allow to discriminate the plant status over the mentioned interfering effects. These effects will be further discussed in the framework of the proposed analysis in 4.5.

For instance, it is worth noting that $R_s(t)$ variations over the long-time scale (hundreds of hours) are also evident in Fig. 5, tough at the raw-data level it is not possible to assess whether these variations arise from the plant growth along the experiment and environmental variations, or from the release of virus-induced VOCs.

As the first step to reduce the dependence from sensor and plant individualities, and to emphasize, for each plant, the variation of the emitted VOCs with respect to the initial condition, sensor features were normalized to the initial conditions of the experiment, i.e. $f_{norm}(t) = (f(t) - f_{ini})/f_{ini}$, where f_{ini} is the mean of the feature values calculated over the first 4 h of stable measurement. Stable means after the stabilization time occurring once the sensor working with temperature modulation is placed inside the bottle containing the target plant.

4.4. Data analysis approach

The time dependence of the plant volatilome composition is a major challenge in this application. Though analytical techniques provide very useful information, a detailed time-resolved knowledge is almost missing. This hinders the precise labelling of the detected atmospheres. Indeed, even if a plant may be considered infected since the time of the inoculation, the volatilome is the real quantity detected by any olfactive technology, and its development may exhibit a complex time-dependence following the dynamics of the plant metabolism [10]. In principle, given this unknown-labels condition, the task of clustering sensor responses into the 'positive-odor' and 'negative-odor' may be addressed by means of unsupervised techniques. We applied methods such as principal component analysis (PCA) and k-Means but we didn't achieve any useful clustering. We retain this result arises from the weak infection-related emission, as compared to the much larger variations induced by effects discussed in 4.3, such as the large humidity and the

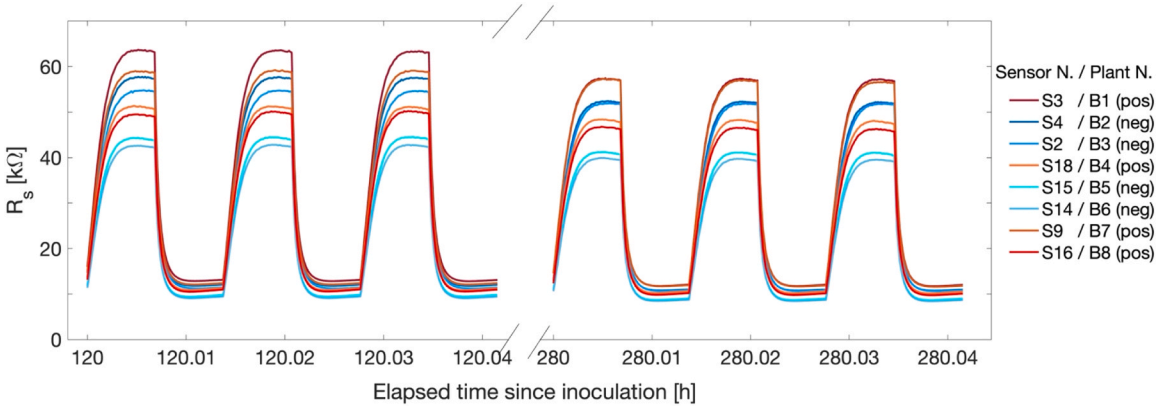

Fig. 5. Overview of raw sensors data. Time dependence of $R_s(t)$ for the sensors employed in session B plotted at two distinct times.

natural plant aging. In these conditions, supervised techniques are more effective than unsupervised ones for discrimination, however they require an a priori knowledge of the proper odor label, which is actually missing. For these reasons we have defined a mathematical function, that we named Δ, which considers the features from the whole network to assess when responses of all sensors exposed to infected plants differ from responses of all sensors exposed to not-infected plants.

To define this function, we refer to Fig. 6 (A), which reports three explanatory cases that may occur during a measurement session with p sensors (from 1 to p) exposed to positive plants and n sensors from ($p+1$ to $n+p$) negative plants. The function is calculated at each measurement time and for each feature, considering all the $n+p$ sensors of the given experimental session. For a given sensor feature we have p feature signals and n feature signals with the same length, defined on the same time base. For the given time t and feature f, the boundaries (minimum and maximum) of the subsets of sensors exposed to positive and negative plants are given by:

$$\min_{pos} = \min\left\{f_1(t), f_2(t), \ldots, f_p(t)\right\}$$

$$\max_{pos} = \max\left\{f_1(t), f_2(t), \ldots, f_p(t)\right\}$$

$$\min_{neg} = \min\left\{f_{p+1}(t), f_{p+2}(t), \ldots, f_{p+n}(t)\right\}$$

$$\max_{neg} = \max\left\{f_{p+1}(t), f_{p+2}(t), \ldots, f_{p+n}(t)\right\}$$

Based on these extremes we may define $\alpha = \max\{\max_{pos}, \max_{neg}\} - \min\{\min_{pos}, \min_{neg}\}$, $\beta = \min\{\max_{pos}, \max_{neg}\} - \max\{\min_{pos}, \min_{neg}\}$, and the function $\Delta = \beta/\alpha$. Its MATLAB® code is reported in the Supplementary Material, 4.

It is worth noting that Δ is defined on the same time base of the features and provides, for each given time, a measure of the distance between the positive and the negative intervals spanned by all the sensors. For example, the three conditions t_0, t_1, t_2, shown in Fig. 6 (A), corresponds to the experimental results reported in Fig. 6 (B) and (C) at $t \approx 186.4$h, $t \approx 122$h, $t \approx 244.4$h, respectively, for $f_{2,norm}$ and $\Delta(f_{2,norm})$ measured in Session B.

Negative values of the function Δ correspond to a complete separation between the two classes (no common intersection) while positive values correspond to a non-zero intersection between the two classes. The more negative the value is, the larger is the separation. The function Δ, calculated feature by feature and for each measurement time, allows to understand which features are suitable to discriminate between the two classes (i.e. are sensible to the VOCs emitted by positive plants) and eventually when differences take place.

4.5. Exploratory data analysis

4.5.1. Features selection and odor-labelling

Fig. 7 shows the functions Δ calculated for all the features listed in Table 1, for session B. The functions Δ can be divided into two groups, one group is given by functions calculated from features 3, 4, 9 (Fig. 7 (A)), while the other group is composed of the functions calculated from the remaining features, Fig. 7 (B). The functions Δ belonging to the first group don't show negative values, except for occasional spikes, while those of the second group show negative values for several time intervals of appreciable length (some hours). This provides an additional criterion for feature selection. Indeed, only features of the second group, namely features 1, 2, 5, 6, 7, 8, differentiate between negative and positive plants and are thus selected for the following analysis. Fig. 7 (B) reports the function Δ of the selected features and shows an interesting oscillation pattern between positive and negative values in the time window

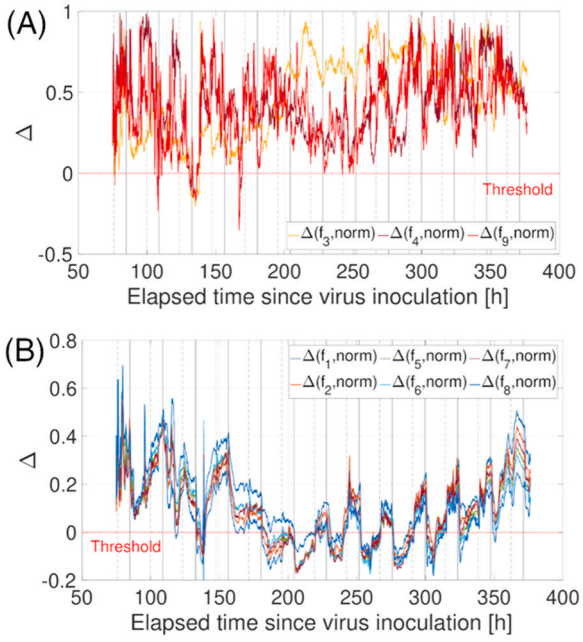

Fig. 7. Functions Δ in session B. (A) functions Δ calculated from the normalized sensor features 3, 4, 9, which are unsuitable to identify the health status of plants. (B) functions Δ for the normalized sensor features 1, 2, 5, 6, 7, 8, which are suitable to identify the health status of plants. Solid and dashed grey lines indicate the start of light- and darkness-periods, respectively.

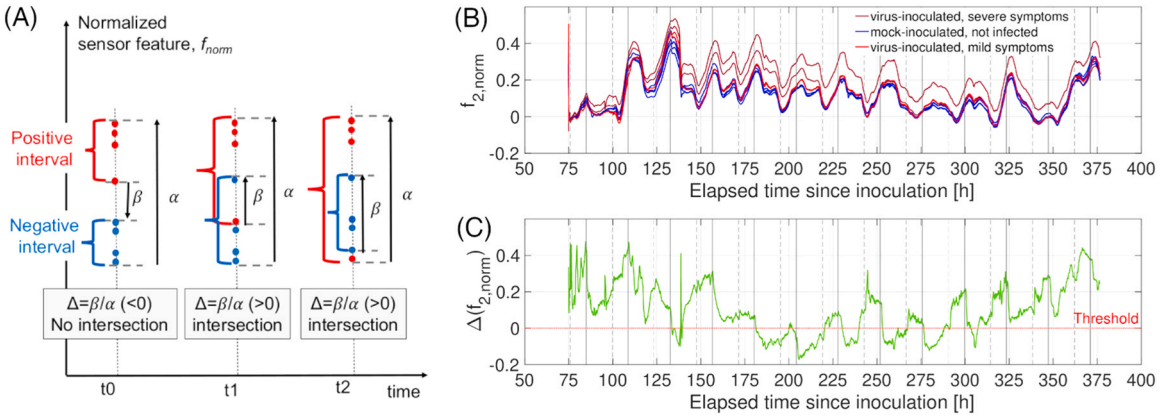

Fig. 6. Explanation of the function Δ. (A) graphical representation of three examples for a given normalized sensor feature $f_{2,norm}$. (B) time dependence of the normalized feature 2 for the 8 sensors used in session B, colors indicate the type of infection and symptoms of the related plants. (C) function Δ calculated from $f_{2,norm}$ reported in (A). In (B) and (C), solid and dashed grey lines indicate the start of light- and darkness-periods, respectively.

approximately from 175 to 325 h post inoculation. Within this time window all the functions Δ decrease quickly after the start of the light period, reaching a minimum at about half of the light period (sometimes before, at about 1/3 of the light period), then increase their value slowly and with the start of the darkness period they increase quickly, reaching positive values. Remembering the meaning of the function Δ, inside that time window the features 1, 2, 5, 6, 7, 8 differentiate between positive and negative plants during the light period and don't during the darkness period. This behavior agrees with the literature of plant volatiles, which reports a light/darkness dependence of the VOCs emission profile [10], and with our GC/MS analysis, which confirmed that no major differences emerge between infected and healthy plants before a period of about 168 h (4.2). We may thus reasonably consider this pattern, namely *the alternation of negative and positive Δ values in correspondendce of the ligh and darkness perids, within the time window of about 175–325 h post inoculation*, as the characteristic comparative pattern of infection.

As an example, Fig. 6 (B) displays $f_{2,norm}$ and the corresponding Δ function. During the daylight separation periods, feature 2 values of positive plants lie above the negative ones, while they decrease and overlap with the negative ones during the darkness periods (except for one positive signal relative to a plant with severe symptoms which stays always above the others).

4.5.2. Humidity and environmental effects

As discussed in 4.3, the large humidity level is a major challenge in this application. However, both *RH* and *T* inside the bottles remain almost constant for the whole experiment, with minimal temperature variations ranging between about 27.8 and 28 °C induced by LED illumination switching on and off (Figure S7 and Figure S8), and equally apply to both healthy and infected plants. So far, even if all these environmental factors are surely playing a role, they are likely to act as a constant bias effect and are not expected to hinder the discrimination capability of the sensor network in our experiment, which is designed as of comparative type.

4.5.3. Plant physiology effects

Concerning the role of plant transpiration, positive dwarf plants feature a smaller surface than negative grown plants (Fig. 3). This will reasonably introduce a difference about transpiration and photosynthesis activity rate and thus in the emission of humidity and oxygen. It could thus be questioned whether the positive/negative difference observed during the light periods effectively arises from the VOCs pattern, or from the different plant surface. However, if the latter case will apply, we shouldn't observe positive values of the function Δ in the last days of the experiment (325–375 h in Fig. 7). To further confirm this, we performed an additional experiment in which sensors exposed to healthy plants, thus subject to transpiration effects, were compared with sensors placed in empty bottles (no plant inside), thus not experiencing transpiration. Figure S9 shows the functions Δ calculated for this experiment, which represent the transpiration pattern. It presents important differences with respect to the pattern of Fig. 7 (B). First, the pattern of Figure S9 is visible since the beginning of the experiment and continues till the end, as it might be reasonably expected from transpiration effects. This differs from Fig. 7 (B), whose pattern occurs in a limited period. Moreover, $f_{3,norm}$ is unsuitable to support the pattern of Fig. 7 but is the best feature for the Figure S9 pattern, showing $\Delta < 0$ during both the light and darkness periods. Yet, $f_{8,norm}$ is meaningful in Fig. 7, but shows $\Delta > 0$ (i.e. no discrimination) for almost the whole experiment of Figure S9. Since different features are generally sensitive to different compounds, this further indicate the different nature of the patterns shown in Fig. 7 and Figure S9. Owing to these arguments, though humidity and the transpiration area certainly play a role, we retain that the Δ-function pattern observed in Fig. 7, namely $\Delta < 0$ during the light periods in the time window approximately from 175 to 325 h post inoculation, reflects the different emission of VOCs by positive and negative plants.

4.5.4. Sensor-to-sensor and plant-to-plant differences

Before to proceed further, it is worth noting that nominally identical sensors may present some differences owing to preparation tolerances. We may further question whether the observed differences between positive and negative plants effectively arise from the infection status of plants or from differences that may distinguish the sensors employed with infected plants from those employed not-infected plants. To rule out this case, the function Δ has been applied to a dataset where the infection-label of a randomly selected positive plant was switched with those of a randomly selected negative plant. Being 4 positive and 4 negative there are 16 possible switching combinations, which are reported in Figure S10. None of the Figure S10 sub-plots show the same light/darkness oscillating pattern of the Δ function observed with the original right labels. This confirms that the pattern of Fig. 7 is related to the difference between positive and negative plants and is not due to sensor to sensor or plant to plant similarities or other external quantities.

With the same aim of confirming the effectiveness of the function Δ to discriminate between infected and not-infected plants we applied it to data of session A (in which inoculation was not effective, as confirmed by RT-qPCR in Fig. 3 (B)). Results are reported in Figure S11, where Δ remains positive for the whole experiment, and the pattern of Fig. 7 (B) is not present at all, thus confirming its correlation with the infection status.

4.5.5. Discriminating healthy and infected plants, concluding remarks

Based on these results and their agreement with GC/MS analysis, Δ can be reasonably considered an indicator of volatile emissions related to the infection status and can thus be used as a reference for the positive-/negative-odor labelling, corresponding respectively to time intervals of $\Delta < 0$ and $\Delta > 0$ respectively.

Fig. 7 further indicates that the proposed technology can detect the infection within about 1 week (180–200 h) since virus inoculation. This detection time may compete with the times of other detection approaches, such as GC/MS (160–200 h, 4.2) and visual inspection (150–170 h, Figure S6). However, the main advantages of MOX sensors rely on their suitability for an automated, in-field operation at a reduced cost, with no need of dedicated personnel, which are hardly compatible with other methods.

It is also worth noting that we worked with Figaro TGS-2620 sensors, however we retain that our results are not unique of this sensor, but other MOX sensors may offer similar performance. Owing to the heterogeneous composition of the target odor, we may reasonably expect that gas sensors featuring broad sensitivity and good responses to one or more key compounds identified in 4.2 should fit to this application. Additionally, we envisage that gas-sensing materials exhibiting a reduced sensitivity to humidity, such as those reported in the dedicated literature [39,41], are likely to be promising for this application.

4.6. Supervised model

4.6.1. Feature selection for the supervised model

The function Δ has been fundamental to investigate when the sensor network detects differences between healthy and infected plants; however, the calculation of Δ requires the a-priori knowledge of the plant status and will not be useful in a real application where the sensor network is deemed to provide this information. To overcome this limitation and develop a suitable model, it is worth noting that all the normalized sensor features 1, 2, 5, 6, 7, 8 selected in 4.4 show the following common characteristics. During $\Delta < 0$ periods, features of positive plants tend to increase faster than those of negative plants at the beginning of the light times, while they tend to decrease faster once the light is switched off (Fig. 6 (B)). These different growth rates are at the base of the separation between the signals of the two classes, which is measured by the Δ.

If positive plants' features will increase more than the negative ones, this means that α (with reference to Fig. 6 (A), α is the total amplitude of

the whole interval) will increase its value after the start of the light period and will decrease after the light has been switched off. This analysis indicates that the key dynamics of the network signals are referred to the beginning of the light and dark period. To properly extrapolate this information, α is thus considered on a day-by-day basis and, for each day, it is normalized to its value at the start of the corresponding light period (Fig. 8). The profile of the normalized α, hereafter called α^*, is conveniently resumed by means of 3 new network features, ϕ_{light}, ϕ_{dark}, ϕ_{diff}, whose definition is reported in Table 2 and schematically shown in Fig. 8 (B). α, and thus α^* and the related ϕ features, does not require any a-priori knowledge about the plant health status and can thus be computed in real-time from the sensors network in the real-scenario application.

4.6.2. Application of the supervised model

Thinking to the real-world scenario, given a network of sensors placed in different points inside a greenhouse, the most likely condition is that the infection outbreak will start from a single plant and so will be registered by only one sensor. To mimic this condition with our data (features values relative to 4 positive and 4 negative plants) we hypothesized to have a network composed of 4 sensing systems placed on 4 different plants. 3 out of 4 plants must be negative, so there are only two possibilities: 3 negatives with a positive (hereafter 3N-1P, this is the case of infection outbreak at a single point, as previously explained) or 4 negative (hereafter 4 N, in this case there is not an infection outbreak). 3N-1P gives a total of 16 different combinations in our experiment (4 combinations for the 3 N and 4 for 1 P, so a total of $4 \times 4 = 16$), while 4 N gives a single possible combination. So far, we have a total of $16 + 1 = 17$ combinations for the considered 4 sensing systems network.

Each of the 17 combinations comprises 12 full days, and there are 5 days with $\Delta < 0$ (labeled as "negative-odor") and 7 days with $\Delta > 0$ (labeled as "positive-odor"). So, the 16 3N-1P combinations give $16 \times 5 = 80$ "negative-odor" days and $16 \times 7 = 112$ "positive-odor" days, while the single combination 4 N provide 5 "negative-odor" days and 7 "positive-odor" days. In total, the input dataset is composed by $80 + 5 = 85$ "negative-odor" days and $112 + 7 = 119$ "positive-odor" days. The dataset size is then $85 + 119 = 204$. As validation scheme, cross-validation with 5 validation folds has been used. For each selected feature two supervised models, KNN and coarse tree, have been trained and validated. Since features $f_{1,2,5,6,7,8\ norm}$ show a similar behavior (Fig. 7 (B)), they are separately tested. Starting from $f_{1,norm}$, the respective α^* and ϕ_{light}, ϕ_{dark}, ϕ_{diff} are calculated as detailed in Table 2 and Fig. 8 (B), and the vector composed by the three ϕ features is used as the input of the supervised algorithm. The same is done for each of the other $f_{2,5,6,7,8\ norm}$ features to compare their performances. Results are summarized in Table 3, referring to the following hyperparameters for KNN: k = 10, distance metrics=euclidean, distance weight=squared inverse, standardize data=yes; and to the following hyperparameters for the coarse tree: maximum numbers of splits= 4, Split criterion=Gini's diversity index, surrogate decision split=off. KNN applied to ϕ features calculated from $f_{1,norm}$ exhibits the largest prediction accuracy (93.1%). Fig. 8 (C) reports the confusion matrix, the false positive and the false negative probabilities are around 10.7% and 3.6% respectively.

Table 2
Network features extracted from the α normalized profile (Fig. 8 (B)).

Feature extracted from the normalized α	Description
Network feature ϕ_{light}	Mean of the normalized α calculated in the 25–33% duration range of the light period
Network feature ϕ_{dark}	Mean of the normalized α calculated in the 17–22% duration range of the dark period
Network feature ϕ_{diff}	$\phi_{light} - \phi_{dark}$

5. Conclusions

In this work, we developed a prototypal sensing system for the non-invasive, on-site, tracking of the health status of tomato plants, using TSWV as target infection. Our system consists of a network of

Table 3
Supervised models prediction accuracy computed for each selected feature listed in Table 1.

Input features	Accuracy weighted KNN	Accuracy Coarse tree
$\phi_{light}(f_{1,norm})$, $\phi_{dark}(f_{1,norm})$, $\phi_{diff}(f_{1,norm})$	93.1%	90.7%
$\phi_{light}(f_{2,norm})$, $\phi_{dark}(f_{2,norm})$, $\phi_{diff}(f_{2,norm})$	87.7%	88.7%
$\phi_{light}(f_{5,norm})$, $\phi_{dark}(f_{5,norm})$, $\phi_{diff}(f_{5,norm})$	89.2%	83.8%
$\phi_{light}(f_{6,norm})$, $\phi_{dark}(f_{6,norm})$, $\phi_{diff}(f_{6,norm})$	87.3%	82.8%
$\phi_{light}(f_{7,norm})$, $\phi_{dark}(f_{7,norm})$, $\phi_{diff}(f_{7,norm})$	89.7%	88.2%
$\phi_{light}(f_{8,norm})$, $\phi_{dark}(f_{8,norm})$, $\phi_{diff}(f_{8,norm})$	81.9%	79.9%

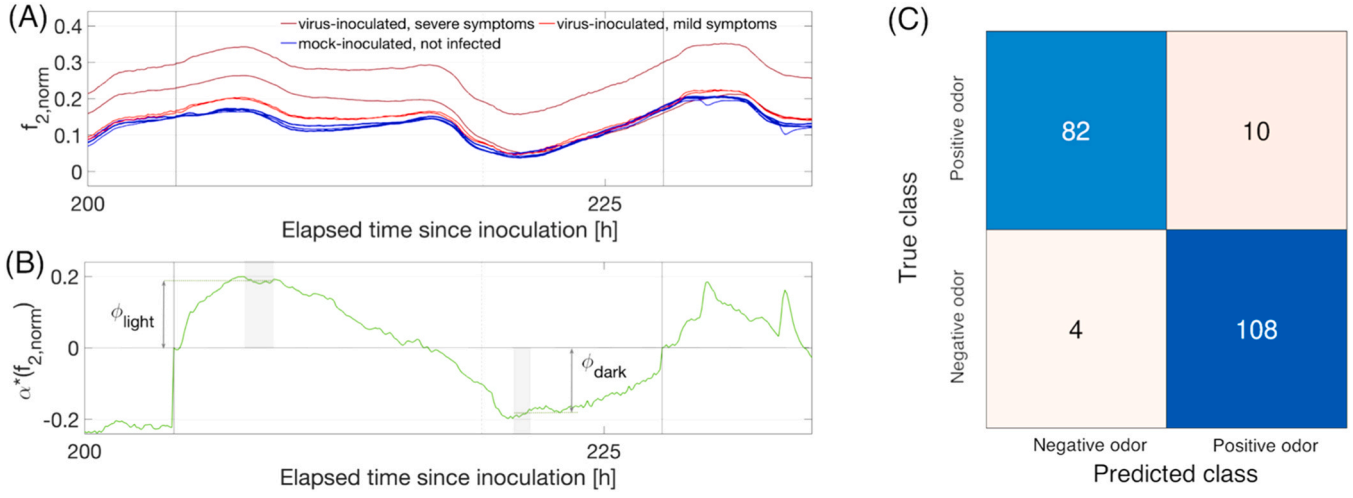

Fig. 8. Development and performance of the KNN model. (A) Detail of the sensors' features $f_{2,norm}$ in the time interval 204–228 h, in session B. (B) Extrapolation of network features ϕ_{light} and ϕ_{dark} from the normalized α (α^*) computed from $f_{2,norm}$. (C) confusion matrix of the KNN model calculated from $\alpha^*(f_{1,norm})$ of session B.

commercial gas sensors based on metal oxides working with temperature modulation, featuring reduced costs and size, suitable to develop a cost-affordable network for in-field operation in greenhouses. To handle issues in sensors' reproducibility and individualities exhibited by different plants, we designed our experiments in sessions considering 8 plants at time, each having a dedicate sensing device, and we developed a data analysis method that exploit features of the whole network, instead of individual sensors. Supported by GC/MS and RT-qPCR analysis, this method allowed us to achieve a reasonable time-resolved labelling of the plants' odors, suitable to train a supervised model. This labelling is fundamental to account for the complex time dependence of VOCs emissions from plants, which depends on the dynamics of plants metabolism and symptoms manifestation. The network, coupled with a supervised model based on KNN, revealed able to detect the outbreak of infection as the occurrence of an anomalous signal from one sensor with respect to the normal trend of the network. These results suggests that metal oxide gas sensors represent a promising technology to develop distributed networks aimed at monitoring the health status of plants in-field.

CRediT authorship contribution statement

Massimo Turina: Writing – review & editing, Supervision, Project administration, Methodology, Investigation, Conceptualization. **Niccolò Miotti:** Writing – review & editing, Investigation. **Carlo Pennacchio:** Writing – review & editing, Writing – original draft, Visualization, Software, Investigation, Formal analysis, Conceptualization. **Andrea Ponzoni:** Writing – review & editing, Writing – original draft, Visualization, Supervision, Software, Project administration, Methodology, Investigation, Formal analysis, Data curation, Conceptualization. **Camilla Baratto:** Writing – review & editing, Supervision, Resources, Funding acquisition. **Guido Faglia:** Writing – review & editing, Supervision, Resources, Funding acquisition. **Gianpiero Vigani:** Writing – review & editing, Supervision, Project administration, Investigation. **Simone Bossi:** Writing – review & editing, Investigation. **Moez Maghrebi:** Writing – review & editing, Investigation. **Emanuela Gobbi:** Writing – review & editing, Supervision, Methodology, Conceptualization. **Marina Ciuffo:** Writing – review & editing, Supervision, Resources, Funding acquisition.

Funding

This research has been partially funded by the European Union – NextGeneration EU, within PRIN 2022, PNRR M4C2, Project "Optical and olfactory sensorial devices to investigate plant-microbe interactions in a model horticultural crop" 2022JZAA9W [CUP: B53D23002700006].

Declaration of Competing Interest

The authors declare that they have no known competing financial interests or personal relationships that could have appeared to influence the work reported in this paper.

Appendix A. Supporting information

Supplementary data associated with this article can be found in the online version at doi:10.1016/j.snb.2026.139921.

Data availability

Data will be made available on request.

References

[1] R.A.C. Jones, Global plant virus disease pandemics and epidemics, Plants 10 (2021) 233, https://doi.org/10.3390/plants10020233.
[2] I.T. Baldwin, R. Halitschke, A. Paschold, C.C. Von Dahl, C.A. Preston, Volatile signaling in plant-plant interactions: "Talking Trees" in the genomics era, Science 311 (2006) 812–815, https://doi.org/10.1126/science.1118446.
[3] R.M.C. Jansen, J. Wildt, I.F. Kappers, H.J. Bouwmeester, J.W. Hofstee, E.J. Van Henten, Detection of diseased plants by analysis of volatile organic compound emission, Annu. Rev. Phytopathol. 49 (2011) 157–174, https://doi.org/10.1146/annurev-phyto-072910-095227.
[4] A. Gbiliy, I. Senosy, M.A.A. Saadan, X. Di, M. Sayed, Y.-Y. Gao, P. Liao, W.M.W. W. Kandegama, M.-Q. Wang, G.-F. Hao, Nanoarchitectures-powered volatile organic compound sensors enable real-time monitoring and early warning in sustainable agriculture, Coord. Chem. Rev. 548 (2026) 217169, https://doi.org/10.1016/j.ccr.2025.217169.
[5] A. Cellini, S. Blasioli, E. Biondi, A. Bertaccini, I. Braschi, F. Spinelli, Potential applications and limitations of electronic nose devices for plant disease diagnosis, Sensors 17 (2017) 2596, https://doi.org/10.3390/s17112596.
[6] R. Spanò, M. Mastrochirico, F. Longobardi, S. Cervellieri, V. Lippolis, T. Mascia, Characterization of volatile organic compounds in grafted tomato plants upon potyvirus necrotic infection, J. Integr. Agric. 22 (2023) 2426–2440, https://doi.org/10.1016/j.jia.2023.02.032.
[7] C. Deng, X. Zhang, W. Zhu, J. Qian, Investigation of tomato plant defence response to tobacco mosaic virus by determination of methyl salicylate with SPME-capillary GC-MS, Chromatographia 59 (2004) 263–268, https://doi.org/10.1365/s10337-003-0144-1.
[8] M. Seskar, V. Shulaev, I. Raskin, Endogenous methyl salicylate in pathogen-inoculated tobacco plants1, Plant Physiol. 116 (1998) 387–392, https://doi.org/10.1104/pp.116.1.387.
[9] V. Shulaev, P. Silverman, I. Raskin, Airborne signalling by methyl salicylate in plant pathogen resistance, Nature 385 (1997) 718–721, https://doi.org/10.1038/385718a0.
[10] R.M.C. Jansen, M. Miebach, E. Kleist, E.J. Van Henten, J. Wildt, Release of lipoxygenase products and monoterpenes by tomato plants as an indicator of *Botrytis Cinerea* -induced Stress, Plant Biol. 11 (2009) 859–868, https://doi.org/10.1111/j.1438-8677.2008.00183.x.
[11] A. Hierlemann, R. Gutierrez-Osuna, Higher-order chemical sensing, Chem. Rev. 108 (2008) 563–613, https://doi.org/10.1021/cr068116m.
[12] T. Liu, L. Guo, M. Wang, C. Su, D. Wang, H. Dong, J. Chen, W. Wu, Review on algorithm design in electronic noses: challenges, status, and trends, Intell. Comput. 2 (2023) 0012, https://doi.org/10.34133/icomputing.0012.
[13] R.M. Cardoso, T.S. Pereira, M.H.M. Facure, D.M. Dos Santos, L.A. Mercante, L.H. C. Mattoso, D.S. Correa, Current progress in plant pathogen detection enabled by nanomaterials-based (Bio)sensors, Sens. Actuators Rep. 4 (2022) 100068, https://doi.org/10.1016/j.snr.2021.100068.
[14] A.T. Güntner, N.J. Pineau, S.E. Pratsinis, Flame-made chemoresistive gas sensors and devices, Prog. Energy Combust. Sci. 90 (2022) 100992, https://doi.org/10.1016/j.pecs.2022.100992.
[15] A. Ponzoni, Metal oxide chemiresistors: a structural and functional comparison between nanowires and nanoparticles, Sensors 22 (2022) 3351, https://doi.org/10.3390/s22093351.
[16] H. Ji, H. Zhu, R. Zhang, H. Gao, Z. Yuan, F. Meng, Suppress ambient temperature interference strategy based on SnO2 gas semiconductor sensor using dynamic temperature modulation mode and principal component analysis algorithm, Sens. Actuators B Chem. 395 (2023) 134543, https://doi.org/10.1016/j.snb.2023.134543.
[17] M. Li, J. Chang, Z. Deng, L. Mi, M. Kumar, S. Wang, Y. He, G. Meng, Discriminating gas molecules at room temperature by UV light modulation (ULM) of nonselective metal oxide sensors, Sens. Actuators B Chem. 378 (2023) 133115, https://doi.org/10.1016/j.snb.2022.133115.
[18] F. Meng, G. Li, H. Ji, Z. Yuan, Investigation on oxygen vacancy regulation mechanism of ZnO gas sensors under temperature modulation mode to distinguish alcohol homologue gases, Sens. Actuators B Chem. 423 (2025) 136747, https://doi.org/10.1016/j.snb.2024.136747.
[19] G.B. Nam, J.-E. Ryu, T.H. Eom, S.J. Kim, J.M. Suh, S. Lee, S. Choi, C.W. Moon, S. J. Park, S.M. Lee, et al., Real-time tunable gas sensing platform based on SnO2 nanoparticles activated by blue micro-light-emitting diodes, Nano-Micro Lett. 16 (2024) 261, https://doi.org/10.1007/s40820-024-01486-2.
[20] B. Zhou, J. Wang, Use of electronic nose technology for identifying rice infestation by nilaparvata lugens, Sens. Actuators B Chem. 160 (2011) 15–21, https://doi.org/10.1016/j.snb.2011.07.002.
[21] R. Ghaffari, F. Zhang, D. Iliescu, E. Hines, M. Leeson, R. Napier, J. Clarkson, Early detection of diseases in tomato crops: An electronic nose and intelligent systems approach. Proceedings of the The 2010 International Joint Conference on Neural Networks (IJCNN), IEEE: Barcelona, Spain, July 2010, pp. 1–6.
[22] A. Cellini, E. Biondi, S. Blasioli, L. Rocchi, B. Farneti, I. Braschi, S. Savioli, M. T. Rodriguez-Estrada, F. Biasioli, F. Spinelli, Early detection of bacterial diseases in apple plants by analysis of volatile organic compounds profiles and use of electronic nose: early detection of bacterial diseases by volatile organic compounds profiling, Ann. Appl. Biol. 168 (2016) 409–420, https://doi.org/10.1111/aab.12272.
[23] S. Cui, E.A.A. Inocente, N. Acosta, HaroldM. Keener, H. Zhu, P.P. Ling, Development of fast e-nose system for early-stage diagnosis of aphid-stressed tomato plants, Sensors 19 (2019) 3480, https://doi.org/10.3390/s19163480.

[24] A.D. Wilson, L.B. Forse, B.A. Babst, M.M. Bataineh, Detection of emerald ash borer infestations in living green ash by noninvasive electronic-nose analysis of wood volatiles, Biosensors 9 (2019) 123, https://doi.org/10.3390/bios9040123.
[25] A. Lee, Temperature modulation in semiconductor gas sensing, Sens. Actuators B Chem. 60 (1999) 35–42, https://doi.org/10.1016/S0925-4005(99)00241-5.
[26] F. Meng, X. Shi, Z. Yuan, H. Ji, W. Qin, Y. Shen, C. Xing, Detection of four alcohol homologue gases by ZnO gas sensor in dynamic interval temperature modulation mode, Sens. Actuators B Chem. 350 (2022) 130867, https://doi.org/10.1016/j.snb.2021.130867.
[27] B. Lee, M. Kang, K. Lee, Y. Chae, K.-J. Yoon, D.-S. Lee, I. Park, Multigas identification by temperature-modulated operation of a single anodic aluminum oxide gas sensor platform and deep learning algorithm, ACS Sens 10 (2025) 954–964, https://doi.org/10.1021/acssensors.4c02715.
[28] H. Ji, Y. Liu, R. Zhang, Z. Yuan, F. Meng, Detection and recognition of toluene and butanone in mixture based on SnO2 sensor via dynamic transient and steady-state response analysis in jump heating voltage mode, Sens. Actuators B Chem. 376 (2023) 132969, https://doi.org/10.1016/j.snb.2022.132969.
[29] H. Ji, C. Mi, Z. Yuan, Y. Liu, H. Zhu, F. Meng, Multicomponent gas detection method via dynamic temperature modulation measurements based on semiconductor gas sensor, IEEE Trans. Ind. Electron 70 (2023) 6395–6404, https://doi.org/10.1109/TIE.2022.3194629.
[30] H. Ji, H. Zhu, R. Zhang, S. Zhang, Z. Yuan, F. Meng, Semiconductor sensor virtual array: gas detection strategy in internet of things to suppress humidity interference, IEEE Internet Things J. 11 (2024) 4934–4941, https://doi.org/10.1109/JIOT.2023.3302408.
[31] A. Ponzoni, A. Depari, E. Comini, G. Faglia, A. Flammini, G. Sberveglieri, Exploitation of a low-cost electronic system, designed for low-conductance and wide-range measurements, to control metal oxide gas sensors with temperature profile protocols, Sens. Actuators B Chem. 175 (2012) 149–156, https://doi.org/10.1016/j.snb.2012.02.018.
[32] V. Krivetskiy, A. Efitorov, A. Arkhipenko, S. Vladimirova, M. Rumyantseva, S. Dolenko, A. Gaskov, Selective detection of individual gases and CO/H2 mixture at low concentrations in air by single semiconductor metal oxide sensors working in dynamic temperature mode, Sens. Actuators B Chem. 254 (2018) 502–513, https://doi.org/10.1016/j.snb.2017.07.100.
[33] G. Zambotti, R. Capuano, V. Pasqualetti, M. Soprani, E. Gobbi, C. Di Natale, A. Ponzoni, Monitoring fish freshness in real time under realistic conditions through a single metal oxide gas sensor, Sensors 22 (2022) 5888, https://doi.org/10.3390/s22155888.
[34] JLM Innovation GmbH Moxstick. ⟨Https://Www.Jlm-Innovation.de/Products/Moxstick⟩ (accessed on 2 December 2025).
[35] P. Margaria, M. Turina, S. Palmano, Detection of flavescence dorée and bois noir phytoplasmas, grapevine leafroll associated virus-1 and -3 and grapevine virus a from the same crude extract by reverse transcription-realtime taqman assays, Plant Pathol. 58 (2009) 838–845, https://doi.org/10.1111/j.1365-3059.2009.02119.x.
[36] P. Margaria, L. Bosco, M. Vallino, M. Ciuffo, G.C. Mautino, L. Tavella, M. Turina, The NSs protein of tomato spotted wilt virus is required for persistent infection and transmission by frankliniella occidentalis, J. Virol. 88 (2014) 5788–5802, https://doi.org/10.1128/JVI.00079-14.
[37] S. Qi, S. Zhang, Md.M. Islam, A.H. El-Sappah, F. Zhang, Y. Liang, Natural resources resistance to tomato spotted wilt virus (TSWV) in Tomato (Solanum lycopersicum), Int. J. Mol. Sci. 22 (2021) 10978, https://doi.org/10.3390/ijms222010978.
[38] P.A. Spencer, G.H.N. Towers, Restricted occurrence of acetophenone signal compounds, Phytochemistry 30 (1991) 2933–2937, https://doi.org/10.1016/S0031-9422(00)98227-X.
[39] H. Kim, A. Haensch, I. Kim, N. Barsan, U. Weimar, J. Lee, The role of NiO doping in reducing the impact of humidity on the performance of SnO_2 -based gas sensors: synthesis strategies, and phenomenological and spectroscopic studies, Adv. Funct. Mater. 21 (2011) 4456–4463, https://doi.org/10.1002/adfm.201101154.
[40] A. Solórzano, R. Rodríguez-Pérez, M. Padilla, T. Graunke, L. Fernandez, S. Marco, J. Fonollosa, Multi-unit calibration rejects inherent device variability of chemical sensor arrays, Sens. Actuators B Chem. 265 (2018) 142–154, https://doi.org/10.1016/j.snb.2018.02.188.
[41] K. Suematsu, M. Sasaki, N. Ma, M. Yuasa, K. Shimanoe, Antimony-doped tin dioxide gas sensors exhibiting high stability in the sensitivity to humidity changes, ACS Sens 1 (2016) 913–920, https://doi.org/10.1021/acssensors.6b00323.

Carlo Pennacchio received the B.Sc. degree in Physics Engineering from Polytechnic of Milano, Italy, in 2020 and the M.Sc. degree in Industrial Automation Engineering from University of Brescia, Italy, in 2022. He has had work experiences both in industry as mechatronics engineer and in research analyzing solid-state gas sensors data. Currently he is a PhD student in micro-nano electronics enrolled at University of Pavia, Italy; his research is about MEMS sensors for applications in harsh environment.

Marina Ciuffo, Degree in Biological Sciences, University of Torino, Italy, in 1996 and Ph. D. degree in Plant Pathology, University of Torino, Italy, in 2009. Presently, she is senior researcher at the Institute for Sustainable Plant Protection of the National Research Council (CNR-IPSP), Torino. Her research interests include the identification and characterization of new plant virus species in vegetable and ornamental crops, studies on virus-plant and virus-vector interaction and characterization of resistance breaking strains; she is also curator of the plant virus collection PLAVIT of IPSP.

Guido Faglia got in 1991 M.S. degree cum laude from the Polytechnic of Milan in electronics. In 1993 he was appointed Assistant Professor at the University of Brescia. In 1996 got the PhD on semiconductor gas sensors. Since 2000 he is Associate Professor in Experimental Physics at University of Brescia. He is involved in the study of preparation of metal oxide semiconductors MOX as thin films and quasi monodimensional nanostructures for gas sensing, energy (solar cells, thermoelectrics), opto-electronic applications (LEDs) and nanomedicine.

Camilla Baratto is a Senior Researcher at CNR-INO, Italy. She has got a M.S. degree in Physics and Ph.D. in Material Science. She is responsible of the CNR-INO Unit of Brescia. With more than twenty years of experience in the realization and testing of both electrical and optical gas sensors, she is also expert in deposition of nanosized semiconductor materials and Raman Spectroscopy. She is Topical Editor of IEEE Sensor Journal.

Andrea Ponzoni received the M.Sc. degree in physics from the University of Parma, Italy, in 2000, and the Ph.D. degree in materials engineering from the University of Brescia, Italy, in 2006. Presently, he is senior researcher at the National Institute of Optics of the National Research Council (CNR-INO), Brescia. His research interests include the investigation of materials for solid-state gas sensors and the development of olfactory systems for application in the fields of agrifood, precision agricultures, safety and security.